

Active Learning via Heteroskedastic Rational Kriging

Shangkun Wang and V. Roshan Joseph*

H. Milton Stewart School of Industrial and Systems Engineering,
Georgia Institute of Technology, Atlanta, GA 30332

July 16, 2025

Abstract

Active learning methods for emulating complex computer models that rely on stationary Gaussian processes tend to produce design points that uniformly fill the entire experimental region, which can be wasteful for functions which vary only in small regions. In this article, we propose a new Gaussian process model that captures the heteroskedasticity of the function. Active learning using this new model can place design points in the more interesting regions of the response surface, and thus obtain surrogate models with better accuracy. The proposed active learning method is compared with the state-of-the-art methods using simulations and two real datasets. It is found to have comparable or better performance relative to other non-stationary Gaussian process-based methods, but faster by orders of magnitude.

Keywords: Computer experiments, Emulation, Gaussian process, Non-stationarity, Sequential design, Surrogate model.

1 Introduction

Computer models are widely used in science and engineering to simulate physical systems. For example, Mak et al. (2018) used large eddy simulations to understand the liquid oxygen flow inside a rocket injector, Krishna et al. (2024) used density functional theory codes to map the potential energy surface of crystal structures, and Huang et al. (2021) used reaction-diffusion models to study the properties of hybrid polymer membranes produced from a vapor phase infiltration process. These computer models are expensive to evaluate, and therefore, they are replaced with easy-to-evaluate surrogate models. Surrogate models

*Corresponding author: roshan@gatech.edu

are created by running computer models using an experimental design and then fitting some statistical models such as kriging or Gaussian process (GP) to the data (Santner et al., 2019; Gramacy, 2020).

Space-filling designs (Joseph, 2016) are widely used as experimental designs for computer experiments. These designs possess some robustness properties and work well over a wide class of computer models. However, it may not be the best experimental design to use for a given computer model. For example, if the computer model is sensitive to the inputs only in a small region of the experimental space and constant everywhere else, then it is wasteful to use a space-filling design to evenly cover the entire experimental region. Better experimental designs for a given computer model can be created using sequential design strategies, also known as active learning. In an active learning strategy, we will start with a small space-filling design, approximately learn about the response surface, and then add points sequentially in regions where the approximation errors are likely to be large.

A crucial step in an active learning strategy is to identify the region where the current surrogate model gives a poor approximation to the true response surface. This is not easy because we do not know the true response surface. This is where the kriging/GP model comes in handy. These models can not only provide a prediction but can also probabilistically quantify the approximation errors. Therefore, their uncertainty estimates can be used to find regions that are likely to have high prediction errors. Although kriging/GP models are widely used for active learning (Gramacy, 2020, Sec. 6.2), they have a major drawback.

To understand the limitation of GP models, consider an underdamped oscillator system shown in Figure 1a. In this system, the moving part oscillates on a rough surface, with its amplitude decreasing exponentially until the system comes to rest. Suppose eight points are sampled using a minimax design, and the data are obtained (shown as gray points in the figure). A GP model (also known as ordinary kriging) can be fitted to this data as follows. Let $y = f(\mathbf{x})$, $\mathbf{x} \in \mathbb{R}^p$ be the true function. Assume a GP prior for the function $f(\mathbf{x}) \sim GP(\mu, \nu^2 R(\cdot))$, where μ is the mean, ν^2 the variance, and $R(\cdot)$ the correlation function defined as $cor\{f(\mathbf{x}_i), f(\mathbf{x}_j)\} = R(\mathbf{x}_i - \mathbf{x}_j)$. Now, given the design $\{\mathbf{x}_1, \dots, \mathbf{x}_n\}$ and the data $\mathbf{Y}_n = [f(\mathbf{x}_1), \dots, f(\mathbf{x}_n)]'$, the posterior distribution of $f(\mathbf{x})$ for a new \mathbf{x} is

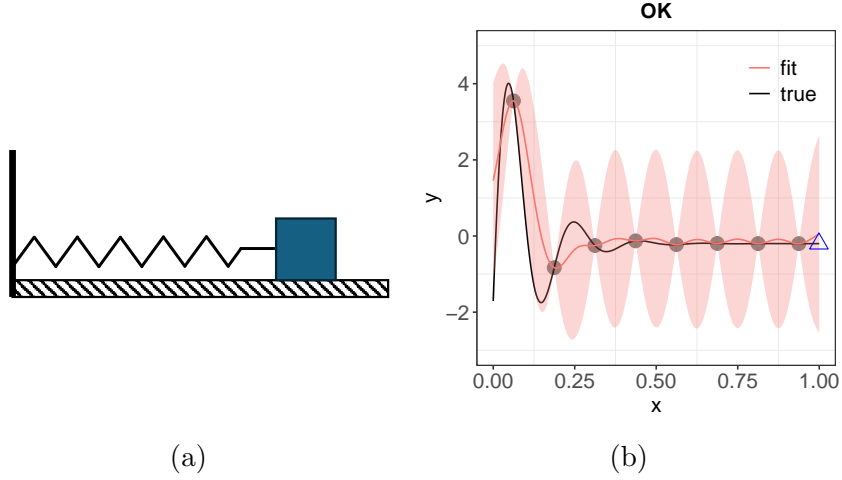


Figure 1: (a) Underdamped oscillator system and its response over time; (b) Ordinary kriging fitted on eight design points denoted as gray. The red solid lines denote the predicted mean and the shaded region is the 95% confidence intervals. Black line is the true response. The blue triangle is the next design point selected by ALM.

given by

$$f(\mathbf{x})|\mathbf{Y}_n \sim \mathcal{N}(\hat{y}(\mathbf{x}), s^2(\mathbf{x})), \quad (1)$$

$$\hat{y}(\mathbf{x}) = \hat{\mu} + \mathbf{r}(\mathbf{x})' \mathbf{R}^{-1}(\mathbf{Y}_n - \hat{\mu} \mathbf{1}_n), \quad (2)$$

$$s^2(\mathbf{x}) = \nu^2 \{1 - \mathbf{r}(\mathbf{x})' \mathbf{R}^{-1} \mathbf{r}(\mathbf{x})\}, \quad (3)$$

where $\mathbf{R} = \{R(\mathbf{x}_i - \mathbf{x}_j)\}_{n \times n}$ is the correlation matrix, $\mathbf{r}(\mathbf{x}) = (R(\mathbf{x} - \mathbf{x}_1), \dots, R(\mathbf{x} - \mathbf{x}_n))'$, $\mathbf{1}_n$ is a vector of 1's, and $\hat{\mu} = \mathbf{1}_n' \mathbf{R}^{-1} \mathbf{Y}_n / \mathbf{1}_n' \mathbf{R}^{-1} \mathbf{1}_n$ is the generalized least squares estimate of μ . Suppose we use a Gaussian correlation function

$$R(\mathbf{u}, \mathbf{v}) = \exp\left(-\sum_{l=1}^p \frac{(u_l - v_l)^2}{\theta_l^2}\right),$$

where $\boldsymbol{\theta} = (\theta_1, \dots, \theta_p)'$ are the lengthscale parameters. Figure 1b shows the predictor $\hat{y}(\mathbf{x})$ (solid red line) and the 95% credible intervals $\hat{y}(\mathbf{x}) \pm 2s(\mathbf{x})$ (shaded region), where the lengthscale parameter is estimated using empirical Bayes methods.

For active learning, it makes sense to sample the next point where the uncertainty is the largest, that is

$$\mathbf{x}_{n+1} = \arg \max_{\mathbf{x} \in \mathcal{X}} s^2(\mathbf{x}), \quad (4)$$

where $\mathcal{X} \subset \mathbb{R}^p$ is the experimental region. As shown in MacKay (1992), this choice maximizes the entropy of the augmented design $\{\mathbf{x}_1, \dots, \mathbf{x}_n, \mathbf{x}_{n+1}\}$. Therefore, in the active learning literature, this strategy is known as Active Learning MacKay (ALM). The ninth point obtained using this strategy is shown in Figure 1b. However, the placement of this point seems counterintuitive. The true function fluctuates more on the left side and is almost flat on the right side. Thus, from the function approximation point of view, we should sample more points on the left side rather than the right side. This is a deficiency of the GP model caused by its stationarity assumption, that is, the function has constant variance throughout the space. This makes the credible intervals roughly the same size, whether it is computed on the left side or on the right side of the function. A closer look at the expression of $s(\mathbf{x})$ also reveals the same issue, which is independent of \mathbf{Y}_n and depends only on how the \mathbf{x}_i 's are distributed. Johnson et al. (1990) shows that a maximum entropy design is asymptotically equivalent to a maximin design. In other words, the ALM strategy will lead to a maximin-type design, which in fact could be worse than the optimal maximin design of the same size due to its one-point-at-a-time myopic construction. Thus, although our aim was to construct a better experimental design using active learning, we ended up in a design that could be much worse than a fixed space-filling design! To be fair, the active learning strategy does have some advantages over a fixed design: (i) we do not need to specify the size of the design beforehand, and we can stop adding points when the approximation is good enough, and (ii) since the lengthscale parameters are learned at each step, the design points will tend to a weighted maximin design which helps to fill the space of important variables. Nevertheless, these advantages are much less than what we had hoped to achieve from active learning.

We can overcome the aforementioned deficiency of the GP model by relaxing the stationarity assumption of variance. Banerjee et al. (2003) proposed to use the model $f(\mathbf{x}) = \mu + \nu(\mathbf{x})Z(\mathbf{x})$, where $Z(\mathbf{x}) \sim GP(0, R(\cdot))$ and $\nu^2(\mathbf{x})$ is a deterministic function that captures heteroskedastic variance. However, it is not easy to postulate a deterministic model for the variance a priori (Ba and Joseph, 2012). Therefore, Huang et al. (2011) proposed to use another GP to model the variance: $\nu^2(\mathbf{x}) = \exp\{\alpha(\mathbf{x})\}$, where $\alpha(\mathbf{x})$ is a GP and the exponential is taken to ensure that the variance will be nonnegative. Extensions of this approach can be found in Tolvanen et al. (2014) and Heinonen et al. (2016). However,

the product of two GPs make the computations challenging. Another approach to model heteroskedasticity is through divide and conquer, where local Gaussian processes are fitted to capture the local variability of the function. Two prominent examples are Treed Gaussian process (Gramacy and Lee, 2008) and local approximate Gaussian process (Gramacy and Apley, 2015). However, the localization introduces discontinuities in the prediction and may not work well unless we have large amounts of data. A yet another approach to introduce non-stationarity is through warped Gaussian process where the input space is transformed, enabling the function to be modeled effectively by a GP in the “warped” space (Sampson and Guttorp, 1992; Schmidt and O’Hagan, 2003). This idea is revived with the deep Gaussian process (DeepGP), which essentially stacks layers of latent GPs together in order to capture complicated non-stationary correlations (Damianou and Lawrence, 2013; Dunlop et al., 2018). Sauer et al. (2023b) used DeepGP for active learning in computer experiments. Another idea to capture nonstationarity is dimension expansion with latent variables (Bornn et al., 2012), which was used for active learning in computer experiments by Montagna and Tokdar (2016). However, these methods use Markov chain Monte Carlo (MCMC) for sampling-based inference, making the prediction and active learning slow, which limits their applicability. Please see Sauer et al. (2023a) for a more comprehensive review of non-stationary GPs.

The main aim of this article is to develop a computationally efficient heteroskedastic GP model and use it to develop an active learning procedure that is fast and easy to use in computer experiments. We extend the recently proposed rational kriging (Joseph, 2024) for this purpose. Rational kriging is computationally efficient and contains enough degrees of freedom to seamlessly integrate heteroskedasticity into the modeling.

The article is organized as follows. Section 2 reviews rational kriging. In Section 3, we propose heteroskedastic rational kriging and develop a computationally efficient procedure for its estimation. Its application to active learning is discussed in Section 4. Section 5 contains extensive simulations to demonstrate the advantages of the proposed procedure compared to the state-of-the-art active learning strategies. Two real case studies are provided in Section 6. We conclude with some remarks in Section 7.

2 Review of Rational Kriging

Joseph (2024) recently proposed a (generalized) rational predictor of the form

$$\hat{y}(\mathbf{x}) = \mu + \frac{\sum_{i=1}^n b_i R(\mathbf{x} - \mathbf{x}_i)}{c_0 + \sum_{i=1}^n c_i R(\mathbf{x} - \mathbf{x}_i)},$$

where $\sum_{i=0}^n c_i^2 = 1$ and $c_i \geq 0$ for all $i = 1, \dots, n$. If $c_0 = 1$, then this reduces to the ordinary kriging (OK) predictor in (2). The rational form of the predictor was motivated by previous work in kriging/GP (Joseph, 2006; Kang and Joseph, 2016) and rational radial basis functions (Jakobsson et al., 2009; Sarra and Bai, 2018; Buhmann et al., 2020). This predictor can be obtained as the posterior mean of a GP of the form:

$$y(\mathbf{x}) = \mu + \tau(\mathbf{x})Z(\mathbf{x}), \quad Z(\mathbf{x}) \sim GP(0, R(\cdot)), \quad (5)$$

where

$$\tau(\mathbf{x}) = \frac{\nu}{c_0 + \mathbf{r}(\mathbf{x})' \mathbf{c}}. \quad (6)$$

Let $\tilde{\mathbf{c}} = (c_0, \mathbf{c}')'$ and $\tilde{\mathbf{R}} = [\mathbf{1}_n, \mathbf{R}]$. Then, the posterior distribution of $y(\mathbf{x})$ given the observations \mathbf{Y}_n can be obtained as

$$y(\mathbf{x}) | \mathbf{Y}_n, \tilde{\mathbf{c}}, \nu, \mu, \theta \sim N(\hat{y}(\mathbf{x}), s^2(\mathbf{x})), \quad (7)$$

where

$$\hat{y}(\mathbf{x}) = \mu + \frac{r(\mathbf{x})'}{c_0 + \mathbf{r}(\mathbf{x})' \mathbf{c}} \mathbf{R}^{-1} \text{diag}(\tilde{\mathbf{R}} \tilde{\mathbf{c}}) (\mathbf{Y}_n - \mu \mathbf{1}_n), \quad (8)$$

and

$$s^2(\mathbf{x}) = \frac{\nu^2}{\{c_0 + \mathbf{r}(\mathbf{x})' \mathbf{c}\}^2} \{1 - \mathbf{r}(\mathbf{x})' \mathbf{R}^{-1} \mathbf{r}(\mathbf{x})\}. \quad (9)$$

If we use a non-informative prior for μ : $p(\mu) \propto 1$, then the posterior distribution of μ is given by

$$\mu | \mathbf{Y}_n, \tilde{\mathbf{c}}, \nu, \theta \sim \mathcal{N} \left(\frac{\tilde{\mathbf{c}}' \tilde{\mathbf{R}}' \mathbf{R}^{-1} \text{diag}(\tilde{\mathbf{R}} \tilde{\mathbf{c}}) \mathbf{Y}_n}{\tilde{\mathbf{c}}' \tilde{\mathbf{R}}' \mathbf{R}^{-1} \tilde{\mathbf{R}} \tilde{\mathbf{c}}}, \frac{\nu^2}{\tilde{\mathbf{c}}' \tilde{\mathbf{R}}' \mathbf{R}^{-1} \tilde{\mathbf{R}} \tilde{\mathbf{c}}} \right). \quad (10)$$

The focus of Joseph (2024) was to improve the estimation of μ . We can see that the posterior variance of μ can be minimized by maximizing the quadratic form $\tilde{\mathbf{c}}' \tilde{\mathbf{R}}' \mathbf{R}^{-1} \tilde{\mathbf{R}} \tilde{\mathbf{c}}$

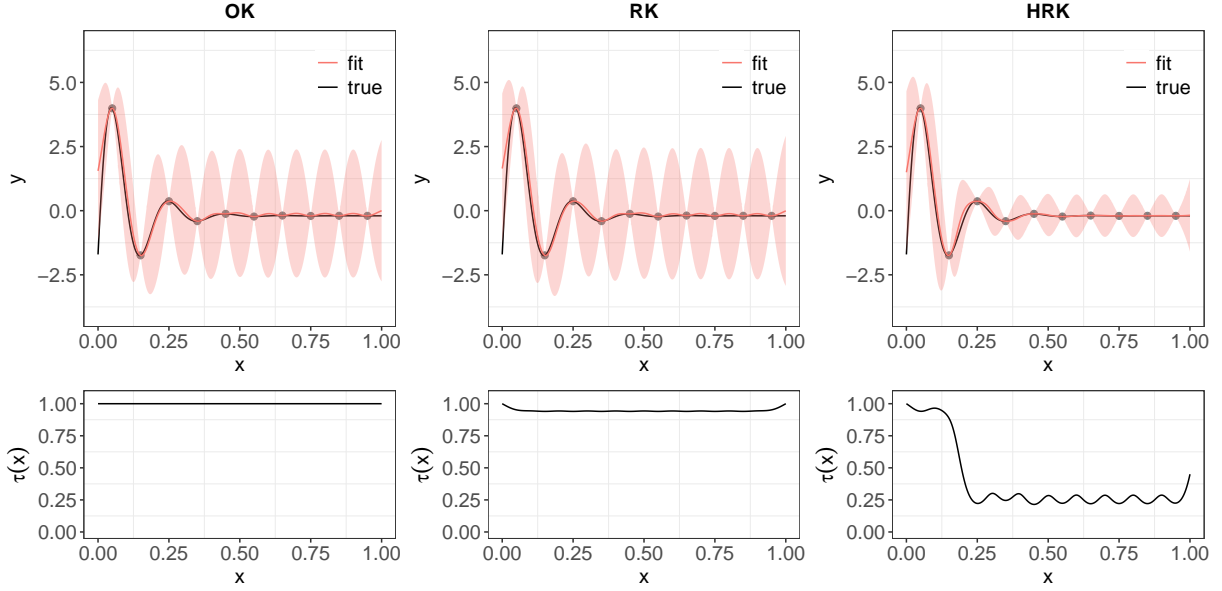


Figure 2: Upper panel: OK, RK and HRK on the underdamped oscillation system. The design is 10 equally spaced points shown in red. The red solid lines denote the predicted mean and the red shaded bands are the 95% confidence intervals. Black line is the true response. Lower panel: the relative variance $\tau(x)$ over the input domain. It is scaled so that the maximum value is 1.

with respect to $\tilde{\mathbf{c}}$ subject to the constraints $\tilde{\mathbf{c}}'\tilde{\mathbf{c}} = 1$ and $\tilde{\mathbf{c}} \geq 0$. This optimization problem has an explicit solution given by the Perron eigenvector of $\tilde{\mathbf{R}}'\mathbf{R}^{-1}\tilde{\mathbf{R}}$.

The middle panels of Figure 2 shows the rational kriging fit and $\tau(\mathbf{x})$ in (6) for the underdamped oscillation system example discussed in the introduction. We can see that the behavior of RK is almost identical to OK in this problem (see the left panels). Therefore, we need to choose $\tilde{\mathbf{c}}$ different from the Perron eigenvector to capture the heteroskedasticity. This is discussed in the next section.

3 Heteroskedastic rational kriging

Since $\tau(\mathbf{x}) = \nu/(c_0 + \mathbf{r}(\mathbf{x})'\mathbf{c})$, we can choose $\tilde{\mathbf{c}} = (c_0, \mathbf{c}')'$ appropriately to model the nonconstant variance of the response surface. This can be done by treating $\tilde{\mathbf{c}}$ as hyperparameters in (5) and jointly estimating them along with the other hyperparameters μ , ν , and $\boldsymbol{\theta}$. To obtain their estimates, we will use empirical Bayes methods, which is common in the analysis of computer experiments (Santner et al., 2019).

The marginal distribution of the data is given by

$$\mathbf{Y}_n | \tilde{\mathbf{c}}, \nu^2, \mu, \boldsymbol{\theta} \sim \mathcal{N}(\mu \mathbf{1}_n, \nu^2 \{\text{diag}(\mathbf{d})\}^{-1} \mathbf{R} \{\text{diag}(\mathbf{d})\}^{-1}), \quad (11)$$

where $\mathbf{d} = (d_1, \dots, d_n)' = \tilde{\mathbf{R}}\tilde{\mathbf{c}} = c_0 \mathbf{1}_n + \mathbf{R}\mathbf{c}$ and $\text{diag}(\mathbf{d})$ is a diagonal matrix with diagonal elements \mathbf{d} . Thus, the maximum likelihood estimates (MLE) of the unknown hyperparameters can be obtained by maximizing

$$\begin{aligned} L &= p(\mathbf{Y}_n | \mathbf{X}_n, \tilde{\mathbf{c}}, \nu^2, \mu, \boldsymbol{\theta}) \\ &\propto \frac{\prod_{i=1}^n d_i}{\nu^n |\mathbf{R}|^{1/2}} \exp \left\{ -\frac{1}{2\nu^2} (\mathbf{Y}_n - \mu \mathbf{1}_n)' \text{diag}(\mathbf{d}) \mathbf{R}^{-1} \text{diag}(\mathbf{d}) (\mathbf{Y}_n - \mu \mathbf{1}_n) \right\} \end{aligned}$$

or equivalently maximizing

$$\begin{aligned} \log L &= -\frac{n}{2} \log \nu^2 + \sum_{i=1}^n \log d_i - \frac{1}{2} \log |\mathbf{R}| \\ &\quad - \frac{1}{2\nu^2} (\mathbf{Y}_n - \mu \mathbf{1}_n)' \text{diag}(\mathbf{d}) \mathbf{R}^{-1} \text{diag}(\mathbf{d}) (\mathbf{Y}_n - \mu \mathbf{1}_n). \end{aligned} \quad (12)$$

Maximizing $\log L$ with respect to μ and ν^2 , we obtain

$$\hat{\mu} = \frac{\mathbf{d}' \mathbf{R}^{-1} \text{diag}(\mathbf{d}) \mathbf{Y}_n}{\mathbf{d}' \mathbf{R}^{-1} \mathbf{d}}, \quad (13)$$

$$\hat{\nu}^2 = \frac{1}{n} (\mathbf{Y}_n - \hat{\mu} \mathbf{1}_n)' \text{diag}(\mathbf{d}) \mathbf{R}^{-1} \text{diag}(\mathbf{d}) (\mathbf{Y}_n - \hat{\mu} \mathbf{1}_n). \quad (14)$$

Plugging them in (12) gives

$$\log L = -\frac{n}{2} \log \hat{\nu}^2 + \sum_{i=1}^n \log d_i - \frac{1}{2} \log |\mathbf{R}| - \frac{n}{2}, \quad (15)$$

which can be maximized with respect $\boldsymbol{\theta}$ and $\tilde{\mathbf{c}}$.

To obtain a fast solution, we will first fit a rational kriging to the data and obtain $\boldsymbol{\theta}_{RK}$. Then we will numerically maximize $\log L$ with respect to $\tilde{\mathbf{c}}$ with $\tilde{\mathbf{c}}_{RK}$ as the initial value. This strategy simplifies the optimization task and enforces some sort of regularization to

obtain a stable solution. Thus, the objective is to

$$\min_{\tilde{\mathbf{c}}} \log \hat{\nu}^2 - \frac{2}{n} \sum_{i=1}^n \log d_i$$

subject to the constraints $\tilde{\mathbf{c}}' \tilde{\mathbf{c}} = 1$ and $\tilde{\mathbf{c}} \geq 0$. This is a high-dimensional optimization with $n + 1$ parameters and should therefore be handled carefully to obtain a computationally efficient solution.

First note that $\hat{\nu}^2$ can also be written as

$$\begin{aligned} \hat{\nu}^2 &= \frac{1}{n} \mathbf{d}' \text{diag}(\mathbf{Y}_n - \hat{\mu} \mathbf{1}_n) \mathbf{R}^{-1} \text{diag}(\mathbf{Y}_n - \hat{\mu} \mathbf{1}_n) \mathbf{d} \\ &= \frac{1}{n} \tilde{\mathbf{c}}' \tilde{\mathbf{R}}' \text{diag}(\mathbf{Y}_n - \hat{\mu} \mathbf{1}_n) \mathbf{R}^{-1} \text{diag}(\mathbf{Y}_n - \hat{\mu} \mathbf{1}_n) \tilde{\mathbf{R}} \tilde{\mathbf{c}} \end{aligned}$$

which is a quadratic function in $\tilde{\mathbf{c}}$ if we fix $\hat{\mu}$ to a reasonable value. Thus, by fixing $\hat{\mu} = \mu_{RK}$, we obtain

$$\hat{\nu}^2 = \frac{1}{n} \{c_0^2 \mathbf{1}'_n \mathbf{Q} \mathbf{1}_n + 2c_0 \mathbf{c}' \mathbf{R} \mathbf{Q} \mathbf{1}_n + \mathbf{c}' \mathbf{R} \mathbf{Q} \mathbf{R} \mathbf{c}\},$$

where $\mathbf{Q} = \text{diag}(\mathbf{Y}_n - \mu_{RK} \mathbf{1}_n) \mathbf{R}^{-1} \text{diag}(\mathbf{Y}_n - \mu_{RK} \mathbf{1}_n)$. Since $c_0 = \sqrt{1 - \mathbf{c}' \mathbf{c}}$, the optimization problem becomes

$$\begin{aligned} \min_{\mathbf{c}} g(\mathbf{c}) &= \log \left(\frac{1}{n} \left\{ (1 - \mathbf{c}' \mathbf{c}) \mathbf{1}'_n \mathbf{Q} \mathbf{1}_n + 2\sqrt{1 - \mathbf{c}' \mathbf{c}} \mathbf{c}' \mathbf{R} \mathbf{Q} \mathbf{1}_n + \mathbf{c}' \mathbf{R} \mathbf{Q} \mathbf{R} \mathbf{c} \right\} \right) \\ &\quad - \frac{2}{n} \mathbf{1}'_n \log \left(\sqrt{1 - \mathbf{c}' \mathbf{c}} \mathbf{1}_n + \mathbf{R} \mathbf{c} \right) \end{aligned} \quad (16)$$

subject to $\mathbf{c}' \mathbf{c} \leq 1$ and $\mathbf{c} \geq 0$,

where $\log \mathbf{x}$ denotes $[\log x_1, \dots, \log x_n]'$. The gradient of $g(\mathbf{c})$ can be explicitly obtained as

$$\begin{aligned} \frac{\partial g}{\partial \mathbf{c}} &= \frac{2}{n \hat{\nu}^2} \left\{ \mathbf{R} \mathbf{Q} \mathbf{R} \mathbf{c} + \sqrt{1 - \mathbf{c}' \mathbf{c}} \mathbf{R} \mathbf{Q} \mathbf{1}_n - \mathbf{1}'_n \mathbf{Q} \mathbf{1}_n \mathbf{c} - \frac{\mathbf{c}' \mathbf{R} \mathbf{Q} \mathbf{1}_n}{\sqrt{1 - \mathbf{c}' \mathbf{c}}} \mathbf{c} \right\} \\ &\quad - \frac{2}{n} \left(\mathbf{R} - \frac{\mathbf{c} \mathbf{1}'_n}{\sqrt{1 - \mathbf{c}' \mathbf{c}}} \right) \{ \text{diag}(\mathbf{d}) \}^{-1} \mathbf{1}_n, \end{aligned}$$

where $\mathbf{d} = \sqrt{1 - \mathbf{c}' \mathbf{c}} \mathbf{1}_n + \mathbf{R} \mathbf{c}$. Now optimization can be carried out efficiently using the globally-convergent method-of-moving-asymptotes (MMA) algorithm (Svanberg, 2002) through the Nlopt package (Johnson, 2008) subject to constraints $\mathbf{c}' \mathbf{c} \leq 1$ and $\mathbf{c} \geq 0$. The

complete algorithm is summarized in Algorithm 1. It is important to note that \mathbf{R} and \mathbf{R}^{-1} are computed only once outside the optimization loop, making this algorithm extremely fast compared to the other nonstationary GPs.

Algorithm 1 HRK Parameter Estimation Procedure

Require: Design points \mathbf{X}_n , response \mathbf{Y}_n

- 1: Fit rational kriging to get $\boldsymbol{\theta}_{\text{RK}}, \mu_{\text{RK}}, \tilde{\mathbf{c}}_{\text{RK}}$;
 - 2: Minimize $g(\mathbf{c})$ in (16) by MMA algorithm with \mathbf{c}_{RK} as the initial value to get $\tilde{\mathbf{c}}$;
 - 3: Calculate $\hat{\mu}$ and $\hat{\nu}^2$ using (13) and (14) respectively;
 - 4: **Return:** $\boldsymbol{\theta}, \hat{\mu}, \tilde{\mathbf{c}}, \hat{\nu}^2$.
-

Our approach is closely related to the maximum likelihood estimation proposed in Kang and Joseph (2016) for an iterated kernel regression. The important differences from their work are that (i) HRK contains c_0 making uncertainty quantification more stable, as shown in Joseph (2024) and (ii) we use a full gradient-based optimization which is extremely fast compared to the iterative nonlinear optimization used in Kang and Joseph (2016).

Consider again the example of an underdamped oscillation system. The prediction and confidence intervals for heteroskedastic rational kriging (HRK) are shown in the top right panel of Figure 2. We can see that the width of the confidence interval provided by HRK is decreasing to the right. The relative variance $\tau(\mathbf{x})$ shown in the bottom right panel exhibits a decreasing trend from 0 to 1, which agrees with our intuition.

To quantitatively compare the performance of different methods, we use two metrics: root mean-squared error (RMSE) to evaluate prediction performance and interval score (IS) (Gneiting and Raftery, 2007) to assess uncertainty quantification. The interval score is defined as

$$IS = \frac{1}{N} \sum_{i=1}^N \left[(u_i - l_i) + \frac{2}{\alpha} \{ (l_i - t_i)_+ + (t_i - u_i)_+ \} \right],$$

where $(x)_+ = x$ if $x > 0$ and 0 otherwise, $[l_i, u_i]$ is the $(1 - \alpha)$ confidence interval, and t_i is the true function values at the i th testing location, $i = 1, \dots, N$. We construct a random Latin hypercube design (LHD) of sizes 10 to 40 and fit RK and HRK. For each design size, we repeat the experiment 10 times. The results are shown as boxplots in Figure 3. It demonstrates that HRK consistently outperforms RK, offering noticeable improvements in both prediction and uncertainty quantification.

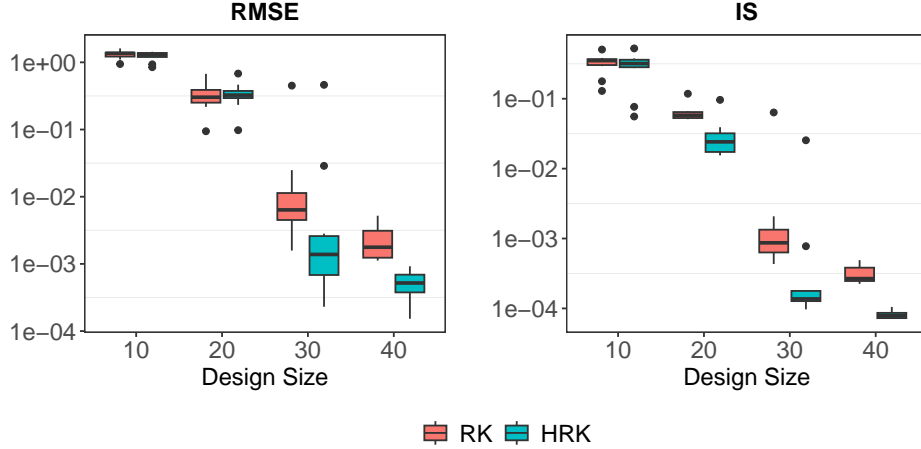


Figure 3: Comparison of RK and HRK as surrogate model for the underdamped oscillation system. Boxplots of RMSE and IS are generated from 10 random Latin hypercube designs of size 10, 20, 30, 40.

4 Active learning

In this section, we will describe the application of heteroskedastic rational kriging (HRK) in active learning. Consider the ALM strategy discussed in the introduction:

$$\mathbf{x}_{n+1} = \arg \max_{\mathbf{x} \in [0,1]^p} \frac{1 - \mathbf{r}(\mathbf{x})' \mathbf{R}^{-1} \mathbf{r}(\mathbf{x})}{\{c_0 + \mathbf{r}(\mathbf{x})' \mathbf{c}\}^2}. \quad (17)$$

The numerator is the same as the variance of OK, which will ensure that the points have a good space-filling property in the space of important variables. The denominator captures the inverse of the variance, which will ensure that the points are placed in regions that are difficult to predict. Thus, HRK enforces these dual objectives in the ALM strategy.

Finding the next design point using (17) involves continuous optimization in p dimensions, which can be time consuming. To simplify optimization, we search for the next design point on a candidate set of size $100(p+1)^2$. This strategy works well as long as we have a good candidate set. For this purpose, we first generate a random Latin hypercube design of size $1000(p+1)^2$ and down-sample it to $100(p+1)^2$ points using the twinning algorithm (Vakayil and Joseph, 2022), which is a quick way to construct a large space-filling design. There are better candidate generation strategies (Wycoff et al., 2024), but they can be slower than the foregoing strategy. The complete algorithm is described in Algorithm 2.

Algorithm 2 Active Learning with HRK

Require: Experiment budget n , initial design size n_{ini} , computer model f .

- 1: Construct initial design $\mathbf{X}_{n_{\text{ini}}}$
 - 2: Evaluate the the responses $\mathbf{Y}_{n_{\text{ini}}} \leftarrow [f(\mathbf{x}_1), \dots, f(\mathbf{x}_{n_{\text{ini}}})]$
 - 3: $\mathbf{D} \leftarrow [(\mathbf{x}_1, y_1), \dots, (\mathbf{x}_{n_{\text{ini}}}, y_{n_{\text{ini}}})]$
 - 4: **for** i in $(n_{\text{ini}} + 1), \dots, n$ **do**
 - 5: Fit HRK on \mathbf{D} by Algorithm 1
 - 6: Generate candidate points \mathbf{X}_{cand}
 - 7: $\mathbf{x}_i = \arg \max_{\mathbf{x} \in \mathbf{X}_{\text{cand}}} s^2(\mathbf{x})$
 - 8: Augment the dataset $\mathbf{D} \leftarrow \mathbf{D} \cup \{(\mathbf{x}_i, y_i)\}$
 - 9: **end for**
 - 10: **Return:** \mathbf{D}
-

Consider again the underdamped oscillation system discussed in the Introduction. The right panel of Figure 4 shows 10 points (blue numbers) selected using Algorithm 2 starting with an initial design of five points (gray points). The same is done using RK and is shown in the left panel of the figure. We can see that the ALM strategy using HRK allocates more points to the left side of the function than that of RK. For example, out of the 10 points, four points are allocated to $x < 0.25$ with HRK, whereas only two points are allocated to the same region with RK. As a result, HRK is able to approximate the function in a better way than RK.

To evaluate HRK’s performance on active learning for the underdamped oscillation example, we compare it against two methods: ordinary kriging using R package: `rkriging` (Huang and Joseph, 2024) and deep Gaussian process using R package: `deepgp` (Booth, 2024). For DeepGP, we adopt a two-layer structure and follow the algorithmic specifications in Sauer et al. (2023b). For all three methods, we initialize the active learning process using a random Latin hypercube design of 10 points and sequentially add 25 points. The results are shown in Figure 5a. We can see that in this example HRK performs better than OK in terms of prediction and uncertainty quantification and also surpasses DeepGP in the end.

A major advantage of HRK is its fast computation compared to other nonstationary GPs. The computational time of HRK, deep Gaussian process, and OK for fixed designs of

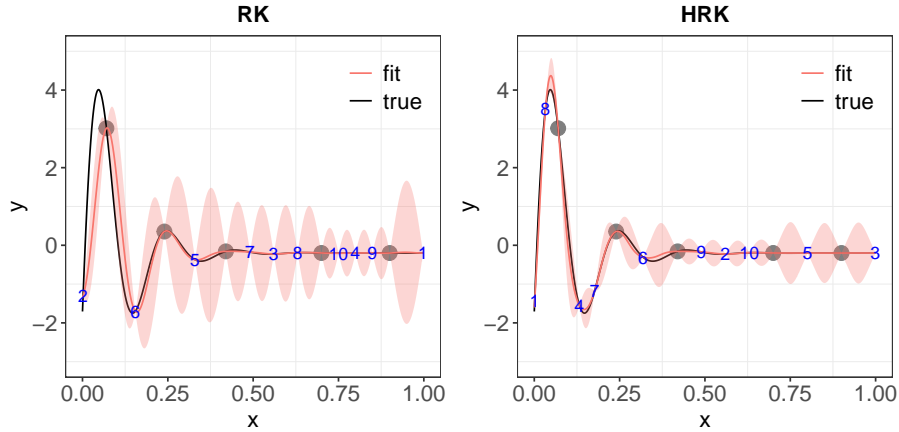


Figure 4: Active learning based on RK and HRK on the underdamped oscillation system. Gray points are the initial 5 design points and blue numbers denotes the next 10 design points selected by ALM. The red solid lines denote the predicted mean and the red shaded bands are the 95% confidence intervals. Black line is the true response.

different sizes is shown in Figure 5b, where the simulation is performed on a 2.6 GHz desktop with 16.0 GB memory. We can see that HRK is more than three orders of magnitude faster than DeepGP and is only slightly slower than OK.

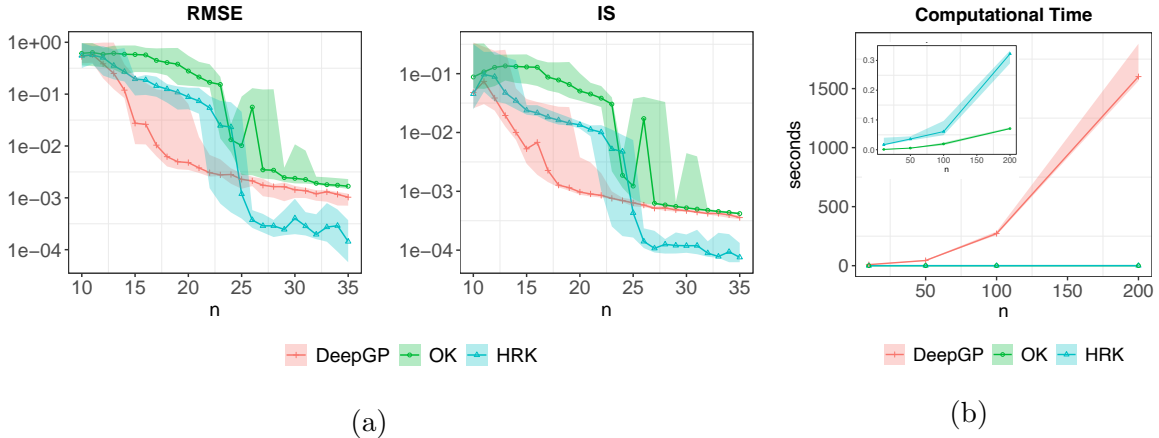


Figure 5: (a) Active learning based on OK, HRK, and DeepGP. The initial designs are random LHDs of size 10. Solid lines represent the median over 10 repetitions and the shaded bands mark the 5th and 95th quantiles. (b) Computational time for fitting DeepGP, HRK, and OK on underdamped oscillation system with n varied from 10 to 200. A zoomed-in view is shown as an inset to see the difference between OK and HRK.

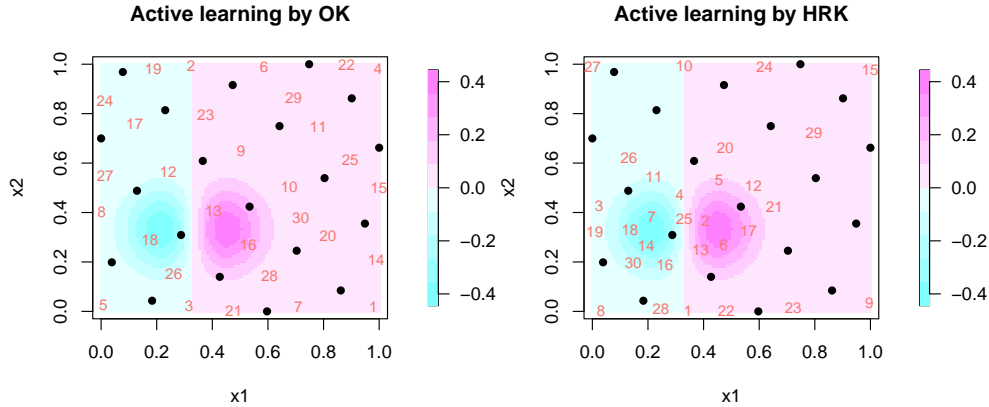


Figure 6: Design points generated using active learning based on ordinary kriging and heteroskedastic rational kriging for the Gramacy-Lee function, where the input domain is scaled to $[0, 1]^2$. The 20 initial points by a MaxPro design are shown as black dots, while the 30 sequentially designed points are labeled as numbers.

5 Simulations

We now investigate the numerical performance of HRK against OK and DeepGP on several test functions. Consider the two-dimensional function from Gramacy and Lee (2009):

$$f(x_1, x_2) = x_1 \exp(-x_1^2 - x_2^2) \quad \text{for } x_1, x_2 \in [-2, 4]. \quad (18)$$

This function exhibits a distinct variation pattern in the domain: it changes rapidly near the lower left corner, whereas the rest of the domain remains relatively flat. Starting with a MaxPro design (Joseph et al., 2015) of 20 points, we add 30 points sequentially using ALM strategy. Figure 6 shows the points obtained using OK (left panel) and HRK (right panel). We can see that the ALM strategy using OK produces points that look almost like a maximin-type space-filling design. On the other hand, HRK allocates more points near the region of high variability, which can lead to better approximation of the response surface.

Now consider some higher-dimensional functions: 8-dimensional Dette-Pepelyshev function (Dette and Pepelyshev, 2010), 4-dimensional cantilever beam function (Eldred et al., 2007), 6-dimensional OTL circuit function (Ben-Ari and Steinberg, 2007), 7-dimensional piston function (Kenett and Zacks, 1998), and 8-dimensional borehole function (Morris et al., 1993). Details of these test functions are available at the Virtual Library of Simula-

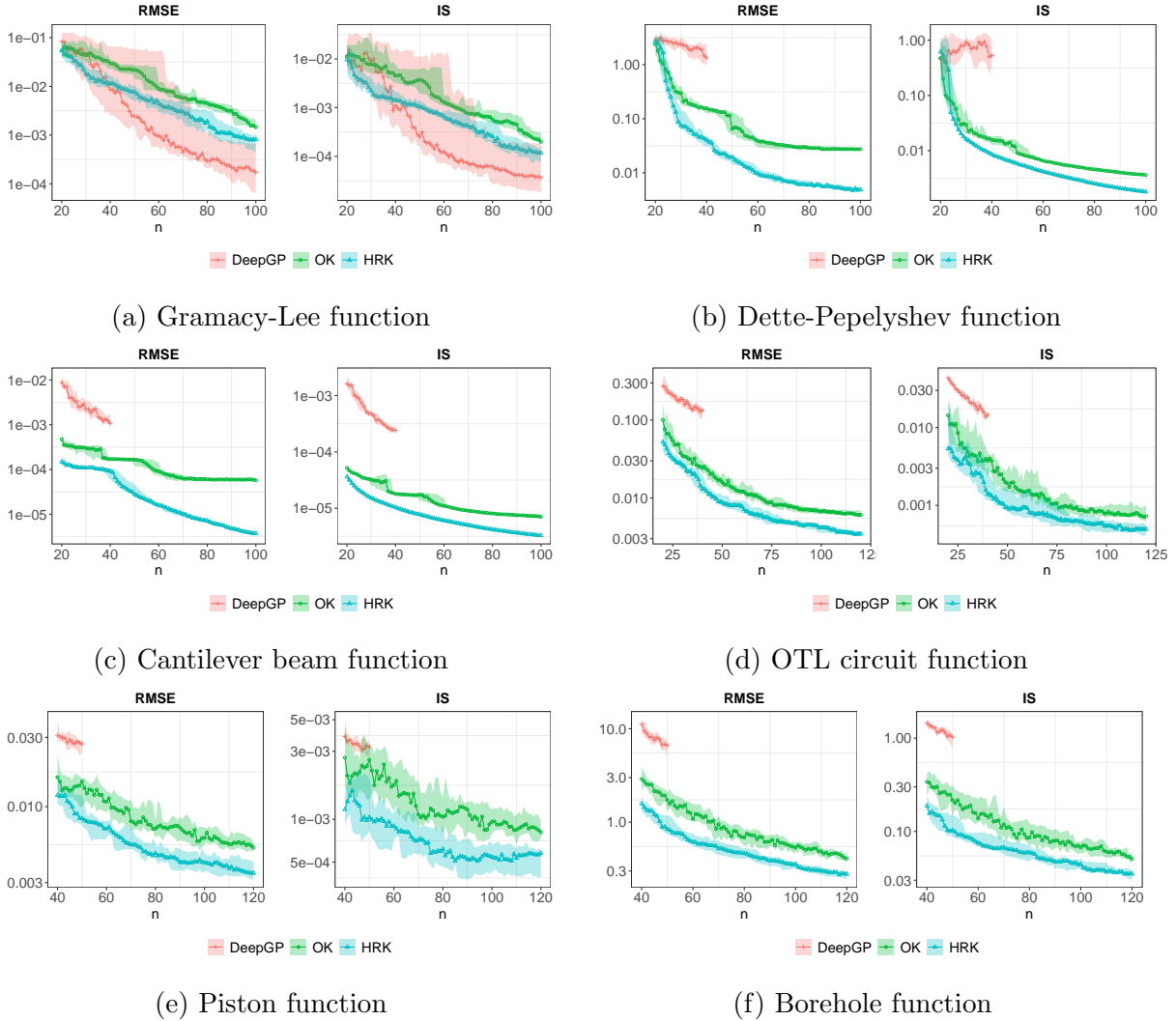


Figure 7: Performance comparison for active learning with HRK, DeepGP and OK. The initial designs are random LHD of size $10p$. Solid lines represent the median over 10 repetitions and the shaded bands mark the 5th and 95th quantiles.

tion Experiments website (Surjanovic and Bingham, 2013).

The results of the simulations with the test functions described above are summarized in Figure 7. DeepGP is run only for a few steps except for the 2-dimensional Gramacy-Lee function due to its high computational time and poor performance. For almost all cases, HRK exhibits improved accuracy over OK. Although DeepGP outperforms HRK in the Gramacy-Lee function, this advantage is not consistent across all scenarios. On the other hand, HRK’s performance seems to be more stable than that of DeepGP. Furthermore, HRK’s simpler structure makes it more interpretable and computationally efficient.

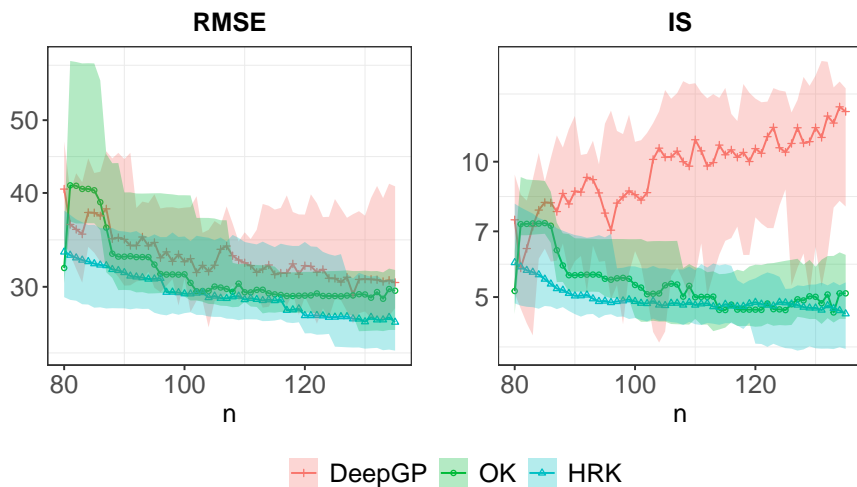


Figure 8: RMSE and IS trajectories for sublimation enthalpy prediction as new molecule structures are selected by active learning.

6 Real Datasets

In this section, we compare the active learning performances of HRK against OK and DeepGP using two real datasets.

6.1 Sublimation Enthalpy Prediction

Sublimation enthalpy (ΔH_{sub}) is a key thermodynamic parameter that quantifies the energy required to sublime a material. It plays a critical role in hybrid membrane process techniques (Leng and Losego, 2017), as it determines the temperature needed to volatilize an organic precursor to achieve a partial pressure suitable for the vapor phase infiltration process. Density Functional Theory (DFT) (Hohenberg and Kohn, 1964) is the state-of-the-art method for calculating sublimation enthalpy with high accuracy. However, its significant computational cost makes it impractical to evaluate every molecule of interest (Lee et al., 2010). The development of comprehensive molecular descriptors/fingerprints for organic compounds and polymers has enabled the use of statistical models trained on DFT data to predict material properties efficiently. A better selection of molecule structures to perform DFT is therefore important for the statistical model to quickly achieve high accuracy.

Liu et al. (2024) generated a dataset comprised of 815 unique organic molecules of interest: <https://khazana.gatech.edu/dataset/>. In order to demonstrate the utility of active learning methods, we will use this dataset to sequentially select structures to run the DFT model for the sublimation enthalpy calculation. The molecular structures are first transformed by a cheminformatics software (RDkit) into descriptors (Landrum, 2006). Five principal components are calculated from these descriptors as input for the following three models: ordinary kriging, deep Gaussian process, and heteroskedastic rational kriging. We start with 80 structures and then sequentially add 55 new structures from the dataset through active learning. The unselected structures are used as test points to evaluate the models’ accuracy. The results are shown in Figure 8, where HRK shows consistent improvement over both OK and deep Gaussian process.

6.2 Langley Glide-Back Booster Dynamics

Langley Glide-Back Booster (LGBB) Dynamics was a project proposed by the National Aeronautics and Space Administration (NASA) to develop a reusable rocket booster (Rogers et al., 2003; Gramacy and Lee, 2009). They aimed to study the flight characteristics (lift, drag, pitch, side-force, yaw, and roll) of the LGBB during atmospheric reentry, with a focus on three key inputs: speed (Mach number), angle of attack (α), and side-slip angle (β). Computational fluid dynamics (CFD) simulations were conducted to explore the rich dynamics under different design configurations.

The dataset is obtained from the lgbb archive at <https://bobby.gramacy.com/surrogates/>. We interpolate the 37,908 data points using Treed Gaussian process (Gramacy and Lee, 2008) and use it as the ground truth. Here we focus only on the lift output, as the other outputs exhibit similar dynamics. We sample 3,000 Sobol points as test locations. All models are trained on a common initial random Latin hypercube design of size 30, and then 40 additional points are selected by Algorithm 2. The results of ten replicated experiments are presented in Figure 9b, where HRK demonstrates a clear improvement over OK in terms of both the RMSE and IS metrics. This could be because, as shown in Figure 9a, lift has a complex transition behavior near the subsonic and supersonic boundary and a small variation throughout the supersonic region. Interestingly, DeepGP did not exhibit a

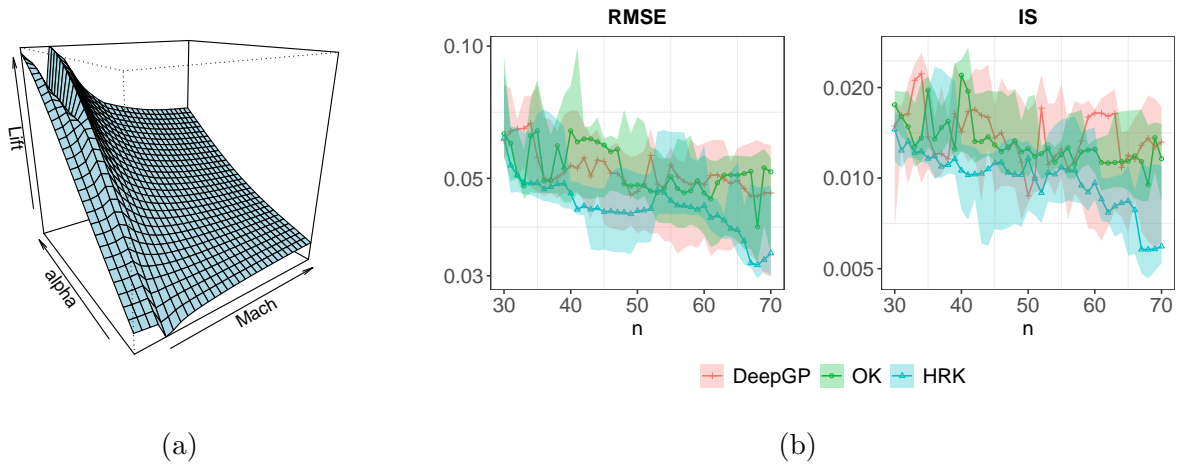


Figure 9: (a) Response surface of the lift as a function of Mach and angle of attack (α) with side-slip angle (β) fixed as 1; (b) RMSE and IS trajectories as new design points are added by active learning.

performance advantage over OK in this scenario, potentially due to suboptimal Bayesian parameter inference.

7 Conclusion

For emulating complex computer models, the main task is to gather data at the right locations in the experimental region so that we can get a good approximation of the response surface. The optimal locations to run the computer codes (optimal experimental design) can be determined based on the potential prediction errors of the emulator (or surrogate model). GP/kriging provides a nice framework for doing this because of its ability to provide uncertainty quantification of prediction errors, which are measured through the posterior variance of the underlying function. Active learning procedures such as ALM work by placing the design points sequentially at locations where the posterior variance is a maximum. Unfortunately, stationarity assumption of variance is commonly employed in GP/kriging, which makes the ALM points behave almost like a maximin-type design, which tends to uniformly fill the entire experimental region. This does not constitute an efficient use of resources because some regions of the response surface can be harder to predict and demand a larger allocation of design points. In this article, we attempted to overcome this deficiency by using a heteroskedastic rational kriging model that captures

the nonconstant variance of the response surface. Simulations with various test functions show that HRK is able to produce comparable or better performance in ALM while being orders of magnitude faster than other nonstationary-based emulation techniques.

This article focuses on active learning procedures for emulation. An important future direction for research is to explore active learning procedures when the objective is optimization. Since HRK is able to provide improved uncertainty quantification, we expect that it will do well in providing a better exploration/exploitation trade-off in the active learning procedures aimed at optimization, but this needs further investigation.

Acknowledgments

This work is supported by U.S. National Science Foundation grants DMREF-1921873 and DMS-2310637.

References

- Ba, S. and Joseph, V. R. (2012), “Composite Gaussian process models for emulating expensive functions,” *The Annals of Applied Statistics*, 1838–1860.
- Banerjee, S., Carlin, B. P., and Gelfand, A. E. (2003), *Hierarchical modeling and analysis for spatial data*, New York, NY: Chapman and Hall/CRC.
- Ben-Ari, E. N. and Steinberg, D. M. (2007), “Modeling data from computer experiments: an empirical comparison of kriging with MARS and projection pursuit regression,” *Quality Engineering*, 19, 327–338.
- Booth, A. S. (2024), *deepgp: Bayesian Deep Gaussian Processes using MCMC*, R package version 1.1.2. available at <https://CRAN.R-project.org/package=deepgp>.
- Bornn, L., Shaddick, G., and Zidek, J. V. (2012), “Modeling nonstationary processes through dimension expansion,” *Journal of the American Statistical Association*, 107, 281–289.
- Buhmann, M. D., De Marchi, S., and Perracchione, E. (2020), “Analysis of a new class of rational RBF expansions,” *IMA Journal of Numerical Analysis*, 40, 1972–1993.

- Damianou, A. and Lawrence, N. D. (2013), “Deep Gaussian processes,” in *Artificial intelligence and statistics*, PMLR, pp. 207–215.
- Detle, H. and Pepelyshev, A. (2010), “Generalized Latin hypercube design for computer experiments,” *Technometrics*, 52, 421–429.
- Dunlop, M. M., Girolami, M. A., Stuart, A. M., and Teckentrup, A. L. (2018), “How deep are deep Gaussian processes?” *Journal of Machine Learning Research*, 19, 1–46.
- Eldred, M., Agarwal, H., Perez, V., Wojtkiewicz Jr, S., and Renaud, J. (2007), “Investigation of reliability method formulations in DAKOTA/UQ,” *Structure and Infrastructure Engineering*, 3, 199–213.
- Gneiting, T. and Raftery, A. E. (2007), “Strictly proper scoring rules, prediction, and estimation,” *Journal of the American statistical Association*, 102, 359–378.
- Gramacy, R. B. (2020), *Surrogates: Gaussian Process Modeling, Design and Optimization for the Applied Sciences*, Boca Raton, FL: Chapman Hall/CRC.
- Gramacy, R. B. and Apley, D. W. (2015), “Local Gaussian process approximation for large computer experiments,” *Journal of Computational and Graphical Statistics*, 24, 561–578.
- Gramacy, R. B. and Lee, H. K. (2009), “Adaptive design and analysis of supercomputer experiments,” *Technometrics*, 51, 130–145.
- Gramacy, R. B. and Lee, H. K. H. (2008), “Bayesian treed Gaussian process models with an application to computer modeling,” *Journal of the American Statistical Association*, 103, 1119–1130.
- Heinonen, M., Mannerström, H., Rousu, J., Kaski, S., and Lähdesmäki, H. (2016), “Non-stationary gaussian process regression with hamiltonian monte carlo,” in *Artificial Intelligence and Statistics*, PMLR, pp. 732–740.
- Hohenberg, P. and Kohn, W. (1964), “Inhomogeneous electron gas,” *Physical review*, 136, B864.
- Huang, C. and Joseph, V. R. (2024), *rkriging: Kriging Modeling*, R package version 1.0. available at <https://CRAN.R-project.org/package=rkriging>.

- Huang, C., Ren, Y., McGuinness, E. K., Losego, M. D., Lively, R. P., and Joseph, V. R. (2021), “Bayesian optimization of functional output in inverse problems,” *Optimization and Engineering*, 22, 2553–2574.
- Huang, W., Wang, K., Jay Breidt, F., and Davis, R. A. (2011), “A class of stochastic volatility models for environmental applications,” *Journal of Time Series Analysis*, 32, 364–377.
- Jakobsson, S., Andersson, B., and Edelvik, F. (2009), “Rational radial basis function interpolation with applications to antenna design,” *Journal of computational and applied mathematics*, 233, 889–904.
- Johnson, M. E., Moore, L. M., and Ylvisaker, D. (1990), “Minimax and Maximin Distance Designs,” *Journal of Statistical Planning and Inference*, 26, 131–148.
- Johnson, S. G. (2008), *The NLopt nonlinear-optimization package*, available at <https://github.com/stevengj/nlopt>.
- Joseph, V. R. (2006), “Limit kriging,” *Technometrics*, 48, 458–466.
- (2016), “Space-filling designs for computer experiments: A review (with discussions),” *Quality Engineering*, 28, 28–44.
- (2024), “Rational Kriging,” *Journal of the American Statistical Association*, available at <https://doi.org/10.1080/01621459.2024.2356296>.
- Joseph, V. R., Gul, E., and Ba, S. (2015), “Maximum projection designs for computer experiments,” *Biometrika*, 102, 371–380.
- Kang, L. and Joseph, V. R. (2016), “Kernel approximation: From regression to interpolation,” *SIAM/ASA Journal on Uncertainty Quantification*, 4, 112–129.
- Kenett, R. and Zacks, S. (1998), *Modern industrial statistics: design and control of quality and reliability*, Pacific Grove, CA: Duxbury Press.
- Krishna, A., Tran, H., Huang, C., Ramprasad, R., and Joseph, V. R. (2024), “Adaptive exploration and optimization of materials crystal structures,” *INFORMS Journal on Data Science*, 3, 68–83.

- Landrum, G. (2006), “RDKit: Open-source cheminformatics. 2006,” available at <https://rdkit.org/>.
- Lee, K., Murray, É. D., Kong, L., Lundqvist, B. I., and Langreth, D. C. (2010), “Higher-accuracy van der Waals density functional,” *Physical Review B—Condensed Matter and Materials Physics*, 82, 081101.
- Leng, C. Z. and Losego, M. D. (2017), “Vapor phase infiltration (VPI) for transforming polymers into organic–inorganic hybrid materials: a critical review of current progress and future challenges,” *Materials Horizons*, 4, 747–771.
- Liu, Y., Tran, H., Huang, C., del Rio, B. G., Joseph, V. R., Losego, M., and Ramprasad, R. (2024), “Accelerated predictions of the sublimation enthalpy of organic materials with machine learning,” *Materials Genome Engineering Advances*.
- MacKay, D. J. (1992), “Information-based objective functions for active data selection,” *Neural computation*, 4, 590–604.
- Mak, S., Sung, C.-L., Wang, X., Yeh, S.-T., Chang, Y.-H., Joseph, V. R., Yang, V., and Wu, C. F. J. (2018), “An efficient surrogate model for emulation and physics extraction of large eddy simulations,” *Journal of the American Statistical Association*, 113, 1443–1456.
- Montagna, S. and Tokdar, S. T. (2016), “Computer emulation with nonstationary Gaussian processes,” *SIAM/ASA Journal on Uncertainty Quantification*, 4, 26–47.
- Morris, M. D., Mitchell, T. J., and Ylvisaker, D. (1993), “Bayesian design and analysis of computer experiments: use of derivatives in surface prediction,” *Technometrics*, 35, 243–255.
- Rogers, S., Aftosmis, M., Pandya, S., Chaderjian, N., Tejnil, E., and Ahmad, J. (2003), “Automated CFD parameter studies on distributed parallel computers,” in *16th AIAA Computational Fluid Dynamics Conference*, p. 4229.
- Sampson, P. D. and Guttorp, P. (1992), “Nonparametric estimation of nonstationary spatial covariance structure,” *Journal of the American Statistical Association*, 87, 108–119.

- Santner, T. J., Williams, B. J., and Notz, W. I. (2019), *The Design and Analysis of Computer Experiments*, New York, NY: Springer.
- Sarra, S. A. and Bai, Y. (2018), “A rational radial basis function method for accurately resolving discontinuities and steep gradients,” *Applied Numerical Mathematics*, 130, 131–142.
- Sauer, A., Cooper, A., and Gramacy, R. B. (2023a), “Non-stationary Gaussian process surrogates,” *arXiv preprint arXiv:2305.19242*.
- Sauer, A., Gramacy, R. B., and Higdon, D. (2023b), “Active learning for deep Gaussian process surrogates,” *Technometrics*, 65, 4–18.
- Schmidt, A. M. and O’Hagan, A. (2003), “Bayesian inference for non-stationary spatial covariance structure via spatial deformations,” *Journal of the Royal Statistical Society Series B: Statistical Methodology*, 65, 743–758.
- Surjanovic, S. and Bingham, D. (2013), *Virtual Library of Simulation Experiments: Test Functions and Datasets*, available at <https://www.sfu.ca/~ssurjano/about.html>.
- Svanberg, K. (2002), “A class of globally convergent optimization methods based on conservative convex separable approximations,” *SIAM journal on optimization*, 12, 555–573.
- Tolvanen, V., Jylänki, P., and Vehtari, A. (2014), “Expectation propagation for nonstationary heteroscedastic Gaussian process regression,” in *2014 IEEE International Workshop on Machine Learning for Signal Processing (MLSP)*, pp. 1–6.
- Vakayil, A. and Joseph, V. R. (2022), “Data twinning,” *Statistical Analysis and Data Mining: The ASA Data Science Journal*, 15, 598–610.
- Wycoff, N., Smith, J. W., Booth, A. S., and Gramacy, R. B. (2024), “Voronoi Candidates for Bayesian Optimization,” *arXiv preprint arXiv:2402.04922*.